Intra- and intercycle interference of electron emissions in laser-assisted XUV atomic ionization

A. A. Gramajo, R. Della Picca, and C. R. Garibotti
Centro Atómico Bariloche, CNEA, and CONICET, 8400 Bariloche, Argentina

D. G. Arbó*
Institute for Astronomy and Space Physics IAFE (CONICET-UBA), Casilla de Correo 67, Sucursal 28, C1428ZAA Buenos Aires, Argentina
(Received 1 August 2016; published 7 November 2016)

We study the ionization of atomic hydrogen in the direction of polarization due to a linearly polarized XUV pulse in the presence of a strong IR laser. We describe the photoelectron spectra as an interference problem in the time domain. Electron trajectories stemming from different optical laser cycles give rise to intercycle interference energy peaks known as sidebands. These sidebands are modulated by a coarse-grained structure coming from the intracycle interference of the two electron trajectories born during the same optical cycle. We make use of a simple semiclassical model that offers the possibility to establish a connection between emission times and the photoelectron kinetic energy. We analyze such interference pattern as a function of the time delay between the IR and the XUV pulses and also as a function of the laser intensity. We compare the semiclassical predictions with the continuum-distorted-wave strong-field approximation and the *ab initio* solution of the time-dependent Schrödinger equation.

DOI: 10.1103/PhysRevA.94.053404

I. INTRODUCTION

New sources of coherent XUV and soft-x-ray radiations delivering pulses with durations in the femtosecond range and with unprecedented high intensities open new perspectives in atomic and molecular physics. Such sources produced from either high-order harmonics or an x-ray free-electron laser (XFEL) pave the way to explore the dynamics of atomic, molecular, and even solid-surface systems undergoing inner-shell transitions. In this way, multiphoton spectroscopy involving synchronized IR and XUV pulses in the strong-field regime can be achieved. The photoelectron spectra from rare-gas atoms have been extensively studied in the simultaneous presence of two pulses from the XUV source and from an IR laser with a time-controlled delay working as a pump-probe experiment [1–3].

The two-color multiphoton ionization where one of the two radiation fields has low intensity and relatively high frequency while the other is intense with a low frequency is usually known as laser-assisted photoemission. Depending on the features of both laser fields (typically the pulse durations), two well-known regimes, the streak camera and sideband, can be distinguished [4–8]. In the former, the XUV pulse is much shorter than the IR period $T_L = 2\pi/\omega_L$, where ω_L is the IR laser frequency and therefore the electron behaves like a classical particle that gets linear momentum from the IR laser field at the instant of ionization [1]. On the other hand, in the latter, where the XUV pulse is longer than the laser period T_L, the photoelectron energy spectrum shows a main line associated with the absorption of one XUV photon accompanied by sideband lines, located more or less symmetrically on its sides. The equally spaced sidebands with separation $\hbar\omega_L$ are associated with an additional exchange of laser photons through absorption and stimulated emission processes. The analysis of the resulting two-color photoelectron spectra can provide information about the high-frequency pulse duration, laser intensity, and the time delay between the two pulses. However, the intermediate situation where the duration of the XUV pulse is comparable to the laser period has not been thoroughly studied.

An accurate theoretical description of the process must be based on quantum mechanical concepts, i.e., by solving *ab initio* the time-dependent Schödinger equation (TDSE) for the atomic system in the presence of the two pulses. However, the precise calculation of the response of a rare-gas atom presents considerable difficulties. The numerical resolution of the TDSE for a multielectron system relies on the single-active-electron approximation, with model potentials that permit one to reproduce the bound-state spectrum of the atom with satisfactory accuracy [9,10]. Models based on a time-dependent distorted-wave theory, such as the strong-field approximation (SFA) and the Coulomb-Volkov approximation, have been extensively employed to study the streaking of the sideband regime transition (see, for example, [11–13]). In the specific sideband regime, where both laser pulse durations are infinite, the soft-photon approximation [14–17] provides a useful description of some general features. However, when discussing the physical content of full numerical results or experimental data where finite-duration pulses are used, it is instructive to compare them to qualitative predictions, such as the simple man's model [18]. Using this semiclassical model for the case of above-threshold ionization (ATI) by one-color lasers, it is possible to identify the photoelectron spectra as the interplay of intra- and intercycle interferences of direct electron trajectories [19,20].

In this paper we extend the semiclassical approximation [19,20] to analyze the laser-assisted photoemission spectra of hydrogen atoms by an XUV pulse, particularly in the intermediate case where $\tau_X \gtrsim T_L$. We show that the role of the IR laser field in the XUV photoionization is threefold: (a) Due to the average wiggling of the electron, it downshifts the energy of the continuum states of the atom by the ponderomotive energy U_p; (b) several IR photons can be absorbed or emitted in the course of the ionization process, giving rise to sidebands (or

*Corresponding author: diego@iafe.uba.ar

intercycle contributions); and (c) it is responsible for intracycle modulations of the sidebands in the photoelectron emission (PE) spectrum. Whereas for (b) we show that the exchange of IR photons in the energy domain can be interpreted as the interference among different electron trajectories emitted by the atom at different optical cycles giving origin to the formation of sidebands, more importantly, the interfering electron trajectories within the same optical cycle give rise to a well-determined modulation pattern encoding information on the ionization process in the subfemtosecond time scale for (c). The same behavior has been observed by Geng *et al.* in [21] for single ionization of He where the contribution of rescattered electrons for single ionization by the IR laser must be considered. By considering two XUV attosecond pulses separated by the laser period they were able to determine intercycle interference, whereas when considering only one XUV attosecond pulse, only the intracycle interference arose.

The paper is organized as follows. In Sec. II we describe the different methods of calculating the photoelectron spectra for the case of laser-assisted XUV ionization: by solving the TDSE *ab initio*, making use of the theory of the SFA, and a semiclassical model (SCM) that gives rise to simple analytical expressions. In Sec. III we present the results and discuss a comparison of results calculated within the different methods. A summary is given in Sec. IV. Atomic units are used throughout the paper, except when stated otherwise.

II. THEORY AND METHODS OF LASER-ASSISTED PHOTOEMISSION

We want to solve the problem of atomic ionization by an XUV pulse in the presence of an IR laser both linearly polarized along the $\hat{z}$ direction. The TDSE in the single-active-electron (SAE) approximation reads

$$i\frac{\partial}{\partial t}|\psi(t)\rangle = H|\psi(t)\rangle, \tag{1}$$

where the Hamiltonian of the system within the dipole approximation in the length gauge is expressed as

$$H = \frac{\vec{p}^{\,2}}{2} + V(r) + \vec{r}\cdot\vec{F}_X(t) + \vec{r}\cdot\vec{F}_L(t). \tag{2}$$

The first term in Eq. (2) corresponds to the active electron kinetic energy, the second term is the potential energy of the active electron due to the Coulomb interaction with the core, and the last two terms correspond to the interaction of the atom with the electric fields $\vec{F}_X(t)$ and $\vec{F}_L(t)$ of the XUV pulse and IR laser, respectively.

As a consequence of the interaction, the bound electron in the initial atomic state $|\phi_i\rangle$ is emitted with momentum $\vec{k}$ and energy $E = k^2/2$ into the final unperturbed state $|\phi_f\rangle$. The photoelectron momentum distributions can be calculated as

$$\frac{dP}{d\vec{k}} = |T_{\rm if}|^2, \tag{3}$$

where $T_{\rm if}$ is the T-matrix element corresponding to the transition $\phi_i \to \phi_f$.

A. Time-dependent Schrödinger equation

In order to numerically solve the TDSE in the dipole approximation for the SAE [Eq. (1)], we employ the generalized pseudospectral method [22–24]. This method combines the discretization of the radial coordinate optimized for the Coulomb singularity with quadrature methods to allow stable long-time evolution using a split-operator representation of the time-evolution operator. Both the bound and the unbound parts of the wave function $|\psi(t)\rangle$ can be accurately represented. Due to the cylindrical symmetry of the system, the magnetic quantum number m is conserved. After the end of the laser pulse the wave function is projected onto eigenstates $|k,\ell\rangle$ of the free atomic Hamiltonian with positive eigenenergy $E = k^2/2$ and orbital quantum number ℓ to determine the transition amplitude $T_{\rm if}$ to reach the final state $|\phi_f\rangle$ (see Refs. [25–27]):

$$T_{\rm if} = \frac{1}{\sqrt{4\pi k}}\sum_{\ell} e^{i\delta_\ell(p)}\sqrt{2l+1}P_\ell(\cos\theta)\langle p,\ell|\psi(t_f)\rangle. \tag{4}$$

In Eq. (4), $\delta_\ell(p)$ is the momentum-dependent atomic phase shift, θ is the angle between the electron momentum $\vec{k}$ and the polarization direction $\hat{z}$, and P_ℓ is the Legendre polynomial of degree ℓ. In order to avoid unphysical reflections of the wave function at the boundary of the system, the length of the computing box was chosen to be 1200 a.u. ($\sim$65 nm) and the maximum angular momentum considered was $\ell_{\rm max} = 200$.

B. Strong-field approximation

Within the time-dependent distorted-wave theory, the transition amplitude in the prior form and length gauge is expressed as

$$T_{\rm if} = -i\int_{-\infty}^{+\infty} dt\,\langle\chi_f^-(\vec{r},t)|[\vec{r}\cdot\vec{F}_X(t) + \vec{r}\cdot\vec{F}_L(t)]|\phi_i(\vec{r},t)\rangle, \tag{5}$$

where $\phi_i(\vec{r},t) = \varphi_i(\vec{r})e^{iI_p t}$ is the initial atomic state with ionization potential I_p and $\chi_f^-(\vec{r},t)$ is the distorted final state. As the SFA neglects the Coulomb distortion in the final channel, the distorted final wave function can be written as $\chi_f^-(\vec{r},t) = \chi^V(\vec{r},t)$, where [28]

$$\chi^V(\vec{r},t) = \frac{\exp\left[i(\vec{k}+\vec{A}(t))\cdot\vec{r}\,\right]}{(2\pi)^{3/2}}\exp\left[\frac{i}{2}\int_t^\infty dt'[\vec{k}+\vec{A}(t')]^2\right] \tag{6}$$

is the length-gauge Volkov state and $\vec{A}(t)$ is the vector potential due to the combined electron field

$$\vec{F}(t) = \vec{F}_L(t) + \vec{F}_X(t). \tag{7}$$

For the sake of simplicity, hereinafter we consider ionization of a hydrogenic atom of nuclear charge $Z = 1$.

C. Semiclassical model

From TDSE and SFA calculations we have observed that for moderate laser intensities the first and second terms in Eq. (5) are well separated in the energy domain: Whereas the single-photon XUV ionization (first term) leads to ionization of electrons with final kinetic energy close to $E \simeq \hbar\omega_X - I_p$

(with ω_X the photon energy of the XUV pulse), the ionization due to the IR laser (second term) leads to electrons with final kinetic energy mostly less than twice its ponderomotive energy $E \lesssim 2U_p$. If we focus on the emission due to the XUV pulse around energy $E \simeq \omega_X - I_p$, the contribution from IR ionization [the second term in Eq. (5)] is negligible when $U_p \ll \omega_X - I_p$. Therefore, inserting Eq. (6) into Eq. (5), the transition amplitude within the SFA reads

$$T_{\rm if} = -i \int_{-\infty}^{+\infty} dt\, \vec{d}(\vec{k} + \vec{A}(t)) \cdot \vec{F}_X(t) \exp\left\{-i \int_t^{\infty} dt' \left[\frac{[\vec{k} + \vec{A}(t')]^2}{2} + I_p\right]\right\}, \quad (8)$$

where the dipole element $\vec{d}(\vec{v})$ is given by

$$\vec{d}(\vec{v}) = \frac{1}{(2\pi)^{3/2}} \int d\vec{r} \exp\left[-i\vec{v}\cdot\vec{r}\,\right] \vec{r}\,\varphi_i(\vec{r}\,). \quad (9)$$

Let us suppose that the XUV pulse has the form $\vec{F}_X(t) = \hat{z} F_{X0}(t) \cos\omega_X t$, where $F_{X0}(t)$ is a slowly nonzero varying envelope function in the time interval with duration τ_X. In this case, writing $\cos\omega_X t = [\exp(i\omega_X t) + \exp(-i\omega_X t)]/2$, the transition amplitude can be written as $T_{\rm if} = T_{\rm if}^{+} + T_{\rm if}^{-}$, where $T_{\rm if}^{+}$ and $T_{\rm if}^{-}$ correspond to the absorption and emission of an XUV photon, respectively. We can discard the emission term since it does not lead to ionization. In other words, according to the rotating-wave approximation, the $T_{\rm if}^{-}$ contribution lies in an energy domain close to $E \simeq -\omega_X - I_p$, which is not in the continuum. Therefore, we can write

$$T_{\rm if} \simeq T_{\rm if}^{+} = -\frac{i}{2} \int_{-\infty}^{+\infty} dt\, d_z(\vec{k} + \vec{A}(t)) F_{X0}(t) \exp[i S(t)], \quad (10)$$

where

$$S(t) = -\int_t^{\infty} dt' \left[\frac{[\vec{k} + \vec{A}(t')]^2}{2} + I_p - \omega_X\right] \quad (11)$$

is the generalized action for the case of laser-assisted photoemission for single XUV photon absorption. As the frequency of the XUV pulse is much higher than the IR laser one, for XUV pulses not much more intense than the IR laser, we can consider the vector potential as due to the laser field only, i.e., $\vec{A}(t) \simeq \vec{A}_L(t)$, neglecting its XUV contribution [29]. In the same way, the ponderomotive energy due to the wiggling of the active electron in the XUV field can be neglected, so $U_p = (F_{L0}/2\omega_L)^2$ for flattop envelopes. If the IR pulse has a nonconstant envelope, a U_p value for each cycle needs to be considered [30].

When the XUV pulse is shorter than the period of the IR laser, i.e., $\tau_X < T_L = 2\pi/\omega_L$, the electron is emitted with kinetic energy that depends on the vector potential at the ionization time, which is known as a streak camera [1,2,4,31]. However, hereinafter, we restrict our analysis to the case where the XUV pulse is comparable to or longer than the period of the IR laser, i.e., $\tau_X \gtrsim T_L$. Specifically, the SCM consists of solving the time integral of Eq. (10) by means of the saddle-point approximation [32–35]. In this sense, the transition probability can be written as a coherent superposition of classical trajectories with the same final momentum $\vec{k}$ as

$$T_{\rm if} = \sum_{t_s} \frac{\sqrt{2\pi}\, F_{X0}(t_s) d_z(\vec{k} + \vec{A}(t_s))}{|[\vec{k} + \vec{A}(t_s)] \cdot \vec{F}_L(t_s)|^{1/2}} \times \exp\left[i S(t_s) + i\frac{\pi}{4} \mathrm{sgn} \frac{d^2 S(t_s)}{dt^2}\right], \quad (12)$$

where from Eq. (11) $d^2S(t_s)/dt^2 = -[\vec{k} + \vec{A}(t_s)] \cdot \vec{F}(t_s)$, sgn denotes the sign function, and t_s are the ionization times corresponding to the stationary points of the action, i.e., $dS(t_s)/dt = 0$. Then, from Eq. (11), the ionization times fulfill the equation

$$\frac{[\vec{k} + \vec{A}(t_s)]^2}{2} + I_p - \omega_X = 0. \quad (13)$$

Let us consider an IR electric field $\vec{F}_L(t) = -F_{L0}\cos(\omega_L t)\hat{z}$, which is a good approximation for long laser pulses where we can neglect the effect of the envelope. The vector potential is thus $\vec{A}(t) = (F_{L0}/\omega_L)\sin(\omega_L t)\hat{z}$. In the following we restrict our analysis to forward emission in the direction of polarization, i.e., $k_z \geqslant 0$ and $k_\rho = 0$ in cylindrical coordinates. Under the condition $F_{L0}/\omega_L < v_0$, where $v_0 = \sqrt{2(\omega_X - I_p)}$ is the electron momentum for ionization of an XUV pulse only, there are two ionization times per optical cycle. They are the early ionization time $t^{(j,1)}$ and the late ionization time $t^{(j,2)}$ corresponding to the jth optical cycle, where $t^{(j,\alpha)} = t^{(1,\alpha)} + 2\pi/\omega_L(j-1)$, with $\alpha = 1,2$ [see Figs. 1(b) and 1(d)]. In order to find the expressions for $t^{(j,\alpha)}$ we must consider two cases, $k_z < v_0$ and $k_z \geqslant v_0$, with solutions

$$t^{(1,1)} = \frac{1}{\omega_L}\sin^{-1}\left[\frac{\omega_L}{F_{L0}}|v_0 - k_z|\right], \quad t^{(1,2)} = \frac{\pi}{\omega_L} - t^{(1,1)} \quad (14)$$

and

$$t^{(1,1)} = \frac{1}{\omega_L}\sin^{-1}\left[\frac{\omega_L}{F_{L0}}|v_0 - k_z|\right] + \frac{\pi}{\omega_L}, \quad t^{(1,2)} = \frac{3\pi}{\omega_L} - t^{(1,1)}, \quad (15)$$

respectively.

Real ionization times are in the framework of classical trajectories of escaping electrons. Equation (13) delimits the classical realm to momentum values $|\frac{\omega_L}{F_{L0}}(k_z - v_0)| < 1$. In other words, the possible classical values of the electron momentum along the positive polarization axis are restricted to $v_0 - F_{L0}/\omega_L \leqslant k_z \leqslant v_0 + F_{L0}/\omega_L$. Outside this domain, ionization times are complex due to the nonclassical nature of such electron trajectories. The imaginary part of these ionization times gives rise to exponentially decaying factors, for which complex (nonclassical) trajectories possess minor relevance compared to real (classical) ones. In consequence, hereinafter we restrict our SCM to classical trajectories.

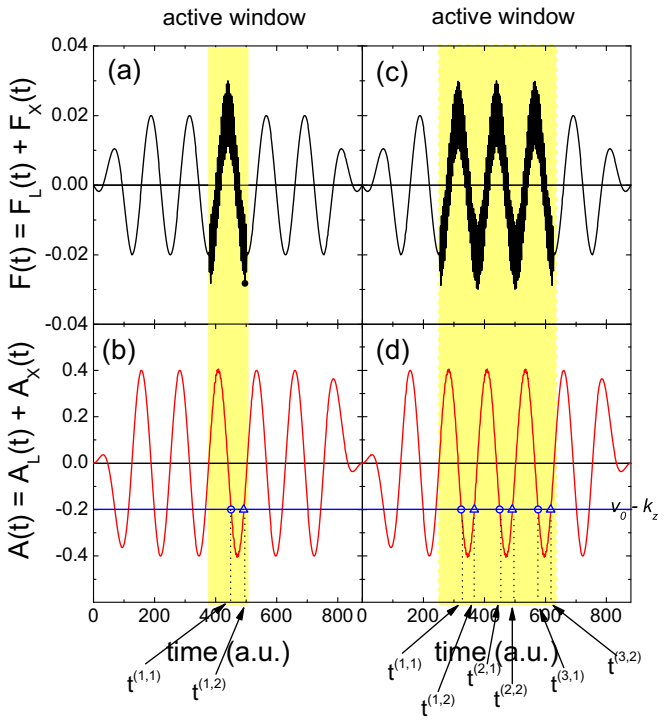

FIG. 1. (a) and (c) Total electric field $F(t) = F_L(t) + F_X(t)$ and (b) and (d) vector potential $A(t) = A_L(t) + A_X(t)$ as a function of time. The IR laser parameters are $F_{L0} = 0.02$, $\omega_L = 0.05$, $\tau_L = 7T_L$, and the XUV pulse with the parameters $F_{X0} = 0.01$ and $\omega_X = 1.5$. The duration of the XUV pulse is (a) and (b) $\tau_X = T_L$ and (c) and (d) $\tau_X = 3T_L$. In (b) and (d) the electron emission early (late) times for a given final momentum k_z are marked by circles (triangles). The shaded area denotes the active time window when XUV ionization takes place.

Including Eq. (12) in Eq. (3), the ionization probability is calculated as

$$|T_{\rm if}|^2 = \left| \sum_{\alpha,j} \frac{\sqrt{2\pi}\, F_{X0}(t^{(j,\alpha)}) d_z(k_z + A(t^{(j,\alpha)}))}{|[k_z + A(t^{(j,\alpha)})] F_L(t^{(j,\alpha)})|^{1/2}} \times \exp\left[i S(t^{(j,\alpha)}) - i \frac{\pi}{4} \mathrm{sgn} F(t^{(j,\alpha)}) \right] \right|^2, \quad (16)$$

with $\alpha = 1$ (2) corresponding to the early (late) release times of Eq. (14) [Eq. (15)]. In Eq. (16), we have stated that v_0 is always positive. Assuming now that the depletion of the ground state is negligible, the ionization rate [the prefactor before the exponential in Eq. (16)] is identical for all subsequent ionization bursts (or trajectories) and is only a function of the time-independent final momentum k_z. This is only valid for the special case that the IR laser is a plane wave with no envelope and the envelope of the XUV pulse $F_{X0}(t)$ is time independent, i.e., flattop pulse, and also for the case where the effect of the Coulomb potential on the receding electron is negligible (SFA). We consider that the flattop XUV pulse comprises an integer number of IR optical cycles, i.e., $\tau_X = NT_L = 2N\pi/\omega_L$. As there are two interfering trajectories per optical cycle of the IR field, the total number of interfering trajectories with final momentum k_z is $2N$, with N being the number of IR cycles involved. The sum over interfering trajectories in Eq. (16) can thus be decomposed into those associated with the two release times within the same cycle and those associated with release times in different cycles. Consequently, the momentum distribution [Eq. (16)] can be written within the SCM as

$$|T_{\rm if}|^2 = \Gamma(k_z) \left| \sum_{j=1}^{N} \sum_{\alpha=1}^{2} \exp\left(i S(t^{(j,\alpha)}) - i \frac{\pi}{4} \mathrm{sgn} F(t^{(j,\alpha)}) \right) \right|^2, \quad (17)$$

where the second factor on the right-hand side describes the interference of the $2N$ classical trajectories with final momentum k_z and $t^{(j,\alpha)}$ is a function of k_z through Eqs. (14) and (15) for $k_z < v_0$ and $k_z \geqslant v_0$, respectively. The ionization probability $\Gamma(k_z)$ is given by

$$\Gamma(k_z) = 2\pi \frac{(F_{X0})^2 |d_z(k_z + A(t^{(j,\alpha)}))|^2}{\left| v_0 F_{L0} \sqrt{1 - \frac{\omega_L^2}{F_{L0}^2}(k_z - v_0)^2} \right|}, \quad (18)$$

where $d_z(\vec{v})$ was defined in Eq. (9).

In the same way as in ionization by an IR laser field alone [19,20] and after a bit of algebra, the sum in Eq. (17) can be written as

$$\sum_{j=1}^{N} \sum_{\alpha=1}^{2} \exp\left(i S(t^{(j,\alpha)} - i \frac{\pi}{4} \mathrm{sgn} F(t^{(j,\alpha)}) \right) = 2 \sum_{j=1}^{N} e^{i\bar{S}_j} \cos\left(\frac{\Delta S_j}{2} - \frac{\pi}{4} \right), \quad (19)$$

where $\bar{S}_j = [S(t^{(j,1)}) + S(t^{(j,2)})]/2$ is the average action of the two trajectories released in the jth cycle and $\Delta S_j = S(t^{(j,1)}) - S(t^{(j,2)})$ is the accumulated action between the two release times $t^{(j,1)}$ and $t^{(j,2)}$ within the same jth cycle. There are two solutions of Eq. (14) [Eq. (15)] per optical cycle: The early release time $t^{(j,1)}$ and the late release time $t^{(j,2)}$ in Eq. (14) [Eq. (15)] lay within the first (or third) quarter of the jth cycle and the second (or fourth) quarter of the jth cycle, respectively.

From Eq. (11), the semiclassical action along one electron trajectory with ionization time $t^{(j,\alpha)}$ can be written, up to a constant, as

$$S(t^{(j,\alpha)}) = \left(\frac{k_z^2}{2} + I_p + \frac{F_{L0}^2}{4\omega_L^2} - \omega_X \right) t^{(j,\alpha)} - \frac{F_{L0}}{\omega_L^2} k_z \cos(\omega t^{(j,\alpha)}) - \frac{F_{L0}^2}{8\omega_L^3} \sin(2\omega t^{(j,\alpha)}). \quad (20)$$

The average action depends linearly on the cycle number j,

$$\bar{S}_j = S_0 + j\tilde{S}, \quad (21)$$

where S_0 is a constant that will be canceled out when the absolute value in Eq. (17) is taken and $\tilde{S} = (2\pi/\omega_L)(E + U_p + I_p - \omega_X)$.

On the other hand, the difference of the action ΔS_j is a constant independent of the cycle number j, which can be

expressed (omitting the subindex j) as

$$\Delta S = \left(\frac{k_z^2}{2} + I_p + U_p - \omega_X\right)\frac{1}{\omega_L} \times \left\{\pi - 2\sin^{-1}\left[\frac{\omega_L}{F_{L0}}|k_z - v_0|\right]\right\} + \mathrm{sgn}(k_z - v_0)\frac{F_{L0}}{2\omega_L^2}(3k_z + v_0)\sqrt{1 - \frac{\omega_L^2}{F_{L0}^2}(k_z - v_0)^2}. \tag{22}$$

We note there is a discontinuity of ΔS at $k_z = v_0$, which is also present in the formalism of Refs. [11,13,36]. This occurs in the present case where the XUV pulse starts at the time t_b so that $A(t_b) = 0$. In general, the discontinuity of ΔS depends on the delay between both pulses. In the next section we show how this discontinuity mirrors the electron emission spectra.

In the same way (after some algebra) as for the case of ionization by a monochromatic pulse [19,20,37,38], Eq. (17) together with Eqs. (19) and (21) can be rewritten as

$$|T_{\mathrm{if}}|^2 = 4\Gamma(k_z)\underbrace{\cos^2\left(\frac{\Delta S}{2} - \frac{\pi}{4}\right)}_{F(k_z)}\underbrace{\left[\frac{\sin(N\tilde{S}/2)}{\sin(\tilde{S}/2)}\right]^2}_{B(k_z)}. \tag{23}$$

This expression indicates that the PE spectrum can be factorized into two different contributions: (i) the interference stemming from a pair of trajectories within the same cycle (*intracycle* interference), governed by the factor $F(k_z)$, and (ii) the interference stemming from trajectories released at different cycles (*intercycle* interference), resulting in the well-known sidebands given by the factor $B(k_z)$. When $N \to \infty$, the intercycle (second) factor becomes a series of δ functions, i.e., $B(k_z) \to \sum_n \delta(E - E_n)$, where

$$E_n = n\omega_L + \omega_X - I_p - U_p \tag{24}$$

are the positions of the sidebands, in agreement with the conservation of energy for the absorption and/or emission of n IR photons and one XUV photon. When $n < 0$ the emission of $|n|$ IR photons is meant, whereas when $n = 0$, the ATI peak for the absorption of only one XUV photon of frequency ω_X is described. It is worth noting that the energy of this ATI peak and all sidebands are shifted with the ponderomotive energy of the IR laser U_p according to Eq. (24). The intracycle interference arises from the superposition of pairs of classical trajectories separated by $\Delta t = t^{(j,2)} - t^{(j,1)}$ of the order of less than half a period of the IR laser pulse, i.e., $\Delta t < \pi/\omega_L$, giving access to an emission time resolution of $\lesssim 1$ fs (for near IR pulses), while the difference between $t^{(j,\alpha)}$ and $t^{(j+1,\alpha)}$ is $2\pi/\omega_L$, i.e., the optical period of the IR laser. Equation (23) is structurally equivalent to the intensity for crystal diffraction: The factor $F(k_z)$ represents the form (or structure) factor accounting for interference modulations due to the internal structure within the unit cell, while the factor $B(k_z)$ gives rise to Bragg peaks due to the periodicity of the crystals. The number N of slits is determined by the duration of the XUV pulse $\tau_X = 2N\pi/\omega_L$. Therefore, $B(k_z)$ in Eq. (23) may be viewed as a diffraction grating in the time domain consisting of N slits with $F(k_z)$ being the diffraction factor for each slit. As in each optical cycle there are two interfering electron trajectories, it is reasonable to obtain a Young-type intracycle interference pattern of the form $F(k_z) = \cos^2(\Delta S/2 - \pi/4)$.

III. RESULTS AND DISCUSSION

In order to compare the different methods described in the preceding section and probe the general conclusion of the SCM that the momentum distribution can be thought as the interplay between the inter- and intracycle interference processes, we consider flattop envelopes for both the IR and XUV pulses for the TDSE and the SFA calculations. In this sense, the IR laser field can be written as

$$\vec{F}_L(t) = F_{L0}(t)\cos\left[\omega_L\left(t - \frac{\tau_L}{2}\right)\right]\hat{z}, \tag{25}$$

where the envelope is given by

$$F_{L0}(t) = F_{L0}\begin{cases}\frac{\omega_L t}{2\pi} & \text{if } 0 \leqslant t \leqslant \frac{2\pi}{\omega_L} \\ 1 & \text{if } \frac{2\pi}{\omega_L} \leqslant t \leqslant \tau_L - \frac{2\pi}{\omega_L} \\ \frac{(\tau_L - t)\omega_L}{2\pi} & \text{if } \tau_L - \frac{2\pi}{\omega_L} \leqslant t \leqslant \tau_L\end{cases} \tag{26}$$

and zero otherwise, so the IR laser field is a cosinelike pulse centered in the middle of the pulse, i.e., $t = \tau_L/2$, where τ_L is the laser pulse duration comprising an integer number of optical cycles with a central flattop region and linear one-cycle ramp on and ramp off.

In the same way, we can define the XUV pulse as

$$\vec{F}_X(t) = F_{X0}(t)\cos\left[\omega_X\left(t - t_{12} - \frac{\tau_L}{2}\right)\right]\hat{z}, \tag{27}$$

with envelope

$$F_{X0}(t) = F_{X0}\begin{cases}\frac{\omega_X t}{2\pi} & \text{if } t_b \leqslant t \leqslant t_b + \frac{2\pi}{\omega_X} \\ 1 & \text{if } t_b + \frac{2\pi}{\omega_X} \leqslant t \leqslant t_e - \frac{2\pi}{\omega_X} \\ \frac{(\tau_X - t)\omega_X}{2\pi} & \text{if } t_e - \frac{2\pi}{\omega_X} \leqslant t \leqslant t_e\end{cases} \tag{28}$$

and zero otherwise. We consider that there is an integer number of optical cycles in the XUV pulse, i.e., $N = \tau_X/2\pi\omega_X$ is a natural number, with a linear one-cycle ramp on and ramp off. The time t_{12} in Eq. (27) characterizes the delay between the centers of the IR and XUV pulses and $t_b = t_{12} + \tau_L/2 - \tau_X/2$ and $t_e = t_{12} + \tau_L/2 + \tau_X/2$ denote the beginning and the end of the XUV pulse, respectively.

In Figs. 1(a) and 1(c) the total electric field $F(t)$ is plotted as a function of time [as defined in Eqs. (7) and (25)–(28)] with IR laser parameters $F_{L0} = 0.02$, $\omega_L = 0.05$, and $\tau_L = 7T_L$ and XUV pulse parameters $F_{X0} = 0.01$ and $\omega_X = 1.5$ with duration $\tau_X = T_L$ in Fig. 1(a) and $\tau_X = 3T_L$ in Fig. 1(c). The XUV pulse opens an active window in the time domain for laser-assisted XUV ionization marked with a yellow shadow in Fig. 1. The definitions of the IR and XUV pulses ensure a flattop vector potential $A(t)$ fulfilling the boundary conditions $A(0) = A(\tau_L) = 0$. In Figs. 1(b) and 1(d) we show the values of $A(t)$ when $\tau_X = T_L$ and $\tau_X = 3T_L$, respectively. They look quite the same since for the chosen parameters the amplitude of the vector potential of the IR laser pulse is $F_{L0}\omega_X/F_{X0}\omega_L = 60$ times higher than the amplitude of the XUV vector potential.

We analyze how the intercycle interference factor $B(k_z)$ and the intracycle interference factor $F(k_z)$ in Eq. (23) control

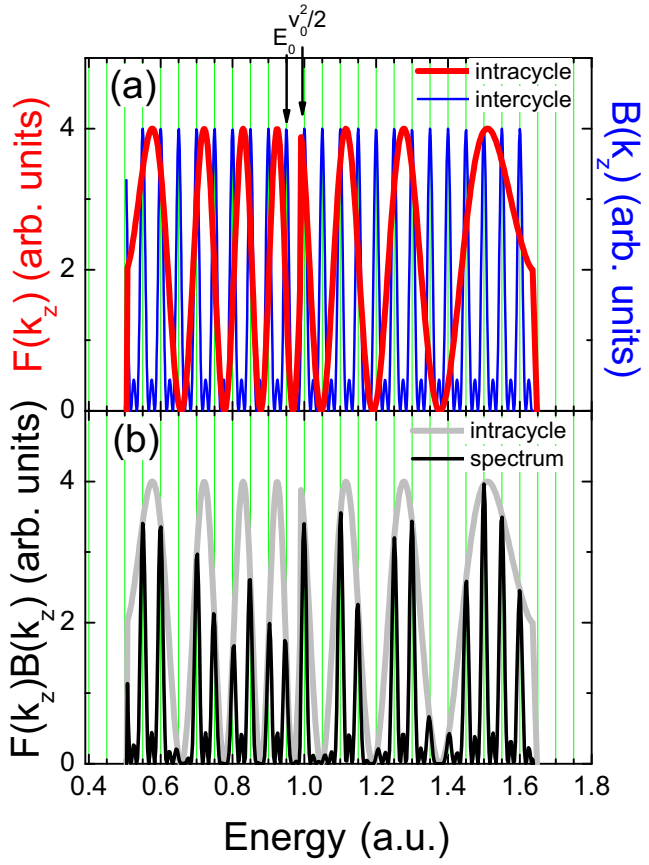

FIG. 2. (a) Buildup of the interference pattern following the SCM. The intracycle pattern is given by the structure pattern $F(k_z)$ in a red thick line and intercycle interference is given by the function $B(k_z)$ with $N = 3$ [Eq. (23)]. (b) Total interference pattern $F(k_z)B(k_z)$ with $N = 3$. The IR laser parameters are $F_{L0} = 0.02$, $\omega_L = 0.05$, the XUV frequency $\omega_X = 1.5$, and delay time $t_{12} = 0$. Both fields are cosinelike. For the sake of comparison, the intracycle pattern $F(k_z)$ of (a) is shown in light gray. Vertical lines depict the positions of the sidebands E_n of Eq. (24).

the electron spectrum for laser-assisted photoemission within the SCM. The factor $B(k_z)$ calculated with the electric field described in Fig. 1(a) is shown in Fig. 2(a) in a (blue) thin line as equispaced peaks with separation between consecutive peaks equal to the IR laser frequency $\hbar\omega_L = 0.05$. The peaks of the function $B(k_z)$ agree perfectly with the energies E_n corresponding to the sidebands [see Eq. (24)] marked with thin vertical lines. Equation (23) predicts $N - 2$ secondary peaks per optical cycle produced by the interference of electron trajectories originated within an active window of N optical cycles (slits) in the laser pulse (diffraction grating). In our case, two minima and a secondary peak are observed due to the interference of three optical cycles ($\tau_x = 3T_L$). The intracycle structure factor $F(k_z)$ shown in the (red) thick curve displays oscillations with maxima unrelated to the sidebands. The positions of these maxima can be calculated with $\Delta S = 2m\pi$, with integer m. The separation of consecutive maxima of the intracycle factor $F(k_z)$ depends on the electron kinetic energy in a nontrivial way, being the separation of the consecutive intracycle maxima higher close to the classical boundaries ($E = 0.51$ and 1.65 a.u.) than at intermediate energies. There is a discontinuity of the difference of the action as a function of energy (and k_z) at $E = v_0^2/2$. According to Eq. (13), ionization times are calculated as the intersection of the horizontal line $v_0 - k_z$ with the vector potential $A(t)$. When $k_z > v_0$, the two ionization times lay in the second half of the optical cycle of the active window [see Fig. 1(b)]. As k_z approaches v_0, the early release time $t^{(1,1)}$ goes to the middle of the active window, whereas the late release time $t^{(1,2)}$ goes to the end of it. In turn, when $k_z < v_0$, the situation is different: As k_z approaches v_0, the early release time $t^{(1,1)}$ goes to the beginning of the active window, whereas the late release times $t^{(1,2)}$ goes to the middle. Such discontinuity does not exist in the case of intracycle interference in above-threshold ionization by one-color pulses since, in that case, $v_0 = 0$ (there is no XUV pulse) in Eq. (22) [19,20,37,38].

In Fig. 2(b) we show the interference pattern for the case of $N = 3$ interfering cycles in the active window [Figs. 1(c) and 1(d)]. Only the factor $B(k_z)F(k_z)$ is displayed, setting the variation of the ionization rate $\Gamma(k_z)$ to unity to focus on the interference process. For the sake of comparison, in light gray, the intracycle pattern $F(k_z)$ of Fig. 2(a) is also displayed. We observe that the intercycle sideband peaks given by $B(k_z)$ [Fig. 2(a)] are modulated by the intracycle interference factor $F(k_z)$. The intracycle interference can lead to the suppression of sidebands (for example, near $E = 1.4$).

We need to compare our SCM with quantum SFA and *ab initio* calculations by solving numerically the TDSE. In Figs. 3(a) and 3(b) we plot the energy distribution of electron emission in the forward direction for the same laser pulse described in Fig. 1 within the SFA and TDSE, respectively, for two different durations of the XUV pulse. In the case of $\tau_X = 3T_L$ we observe a set of peaks separated by the laser frequency ω_L, in agreement with Eq. (24), whose positions are pointed with vertical thin lines. By comparing Figs. 2 and 3 we see that the quantum (TDSE and SFA) energy distributions extend about 0.2 a.u. beyond the classical limits $(v_0 \mp F_{L0}/\omega_L)^2/2$. The agreement between SFA and TDSE results is remarkable and both are qualitatively similar to the SCM of Fig. 2. We would like to point out that the energy distributions exhibit sharp modulations, in agreement with the intracycle interference pattern calculated with an XUV pulse duration $\tau_X = T_L$, in a gray thick line. In this sense, the fact that the intracycle interference pattern modulates the sidebands in the energy distribution, albeit derived within the SCM, is also valid for the quantum calculations. The reason for this is under current investigation, however, we note that it is closely related to previous works [11–13] where the PE spectrum is factorized as two contributions as in Eq. (23). It is also worth mentioning that, as within the SCM, in the SFA and the TDSE PE spectra there are frustrated sidebands, close to $E = 0.63$, 1.03, 1.2, and 1.4 coinciding with the minima of the intracycle interference pattern.

In what follows we compare the SCM with similar approximations based on the SFA, like in the works of Kazansky *et al.* [11,12], Bivona *et al.* [13], and the soft-photon approximation [14]. The authors of [11–13] have also employed the saddle-point approximation to obtain analytical expressions for photoelectron spectrum giving rise to the factorization of the different contributions, i.e., the intra- and intercycle interferences. Our results are in good agreement

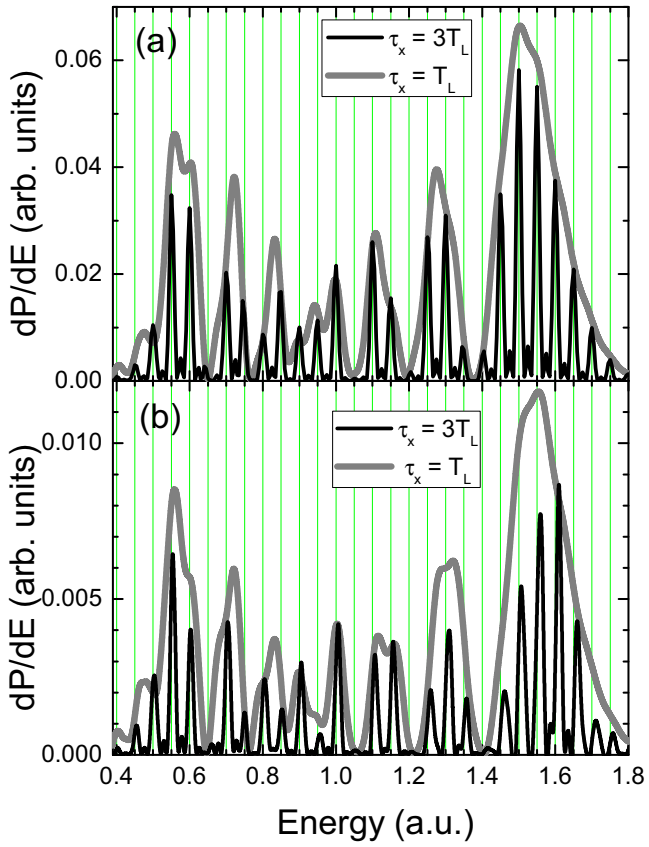

FIG. 3. Energy distribution in the forward direction for the same laser parameters and XUV frequency as in Fig. 1 calculated within (a) the SFA and (b) the TDSE. The laser duration is $\tau_L = 7T_L = 879.65$ and the XUV field amplitude $F_{X0} = 0.01$. Vertical lines depict the positions of the sidebands E_n in Eq. (24).

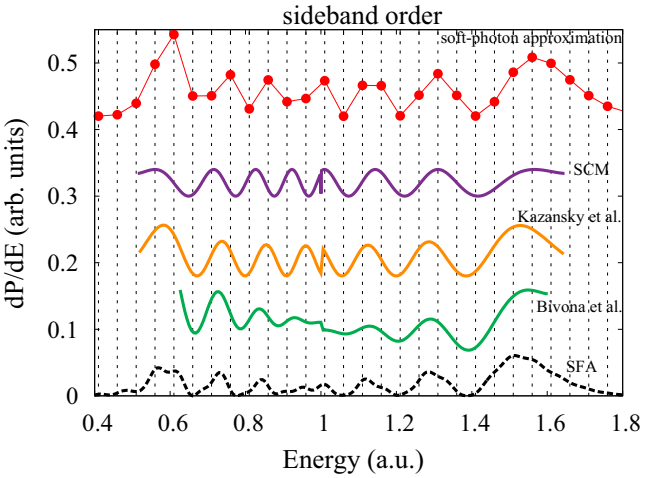

FIG. 4. Photoelectron spectra in the forward direction (in arbitrary units) for time delay $t_{12} = 0$ for the SFA (black dashed line), the approximation of Bivona *et al.* [13] (green solid line), the approximation of Kazansky *et al.* [11,12] (orange solid line), the semiclassical model (purple solid line), and the soft-photon approximation (thin red solid line with circles). The IR laser parameters are $F_{L0} = 0.02, \omega_L = 0.05, \tau_L = 7T_L$, and the XUV pulse with the parameters $F_{X0} = 0.01$, $\omega_X = 1.5$, and duration $\tau_X = T_L$. Both fields are cosinelike.

with previous works [11–13]. Our intracycle factor $F(k_z)$ in Eq. (23) matches exactly with the first-order prediction of Kazansky *et al.* In Fig. 4 we compare the SCM, SFA, soft-photon approximation, and results obtained by application of Eq. (15) of [11,12] and Eq. (25) of [13]. We observe that the discontinuity at $E_{\rm disc} = 1$ for the SCM is also present for the results of Kazansky *et al.* and Bivona *et al.*, whereas the soft-photon approximation predicts only the height of the sidebands due to the infinite pulse durations considered in that theory. We want to point out that the soft-photon approximation in Fig. 4 was modified with respect to Eq. (12) of [14] in order to include the ponderomotive shift, so the sideband positions are at the positions in Eq. (24), in agreement with the energy conservation. The agreement between the SCM and the other approximations, including the SFA, is very good since not only does it predict the same number of maxima on both sides of the zeroth-order sideband but also their positions are well reproduced.

In order to investigate the dependence of the intracycle interference pattern on the laser intensity, we show in Fig. 5 calculations of the energy distribution in the forward direction within the SCM [Fig. 5(a)], the SFA [Fig. 5(b)], and the TDSE [Fig. 5(c)], for laser field amplitudes from $F_{L0} = 0$ up to 0.05. In this sense, the intracycle pattern in Figs. 2(a), 3(a), and 3(b) are cuts at $F_{L0} = 0.02$ of Figs. 5(a), 5(b), and 5(c), respectively. The classical boundaries $(v_0 \mp F_{L0}/\omega_L)^2/2$ are drawn as dashed lines and they exactly delimit the SCM spectrogram of Fig. 5(a), as expected. Figure 5(a) shows that the discontinuity at $E = v_0^2/2 = 1$ is clearly independent of the laser field amplitude. Above the discontinuity, the interference maxima (and minima) exhibit a positive slope as a function of F_{L0}, whereas below it, the stripes have negative slope. The boundaries slightly blur for the SFA spectrogram, also showing the characteristic intracycle stripes with positive (negative) slope close to the top (bottom) classical boundary, however, missing the SCM discontinuity at $E_{\rm disc}$. In Fig. 5(c) the TDSE calculation exhibits a strong probability distribution for high values of F_{L0} in the low-energy region. The source of this enhancement of the probability is the atomic ionization by the IR laser pulse alone, which has not been considered in our SCM and is strongly suppressed in the SFA because the laser photon energy is much lower than the ionization potential, i.e., $\omega_L \ll I_p$. For this reason we can confirm that the SFA is a very reliable method to deal with laser-assisted photoemission rather than ATI by IR lasers. Except for the region where ionization by the laser field alone becomes important, SFA and TDSE spectrograms agree with each other and qualitatively resemble the SCM calculations.

So far, we have performed our analysis for the electron emission in the forward direction for zero time delay $t_{12} = 0$, i.e., the center of the IR laser and XUV pulses coincide. In order to reveal how the intracycle interference pattern changes with the time delay, we vary t_{12} from 0 up to T_L. This means that the center of the XUV pulse shifted by t_{12} with respect to the center of the IR pulse corresponds to a phase in the laser optical cycle $\phi = \omega_L t_{12} = 2\pi t_{12}/T_L$. In Fig. 6(a) we show the SCM intracycle interference pattern in the forward direction as a function of the optical phase or time delay t_{12}. The horizontal stripes show

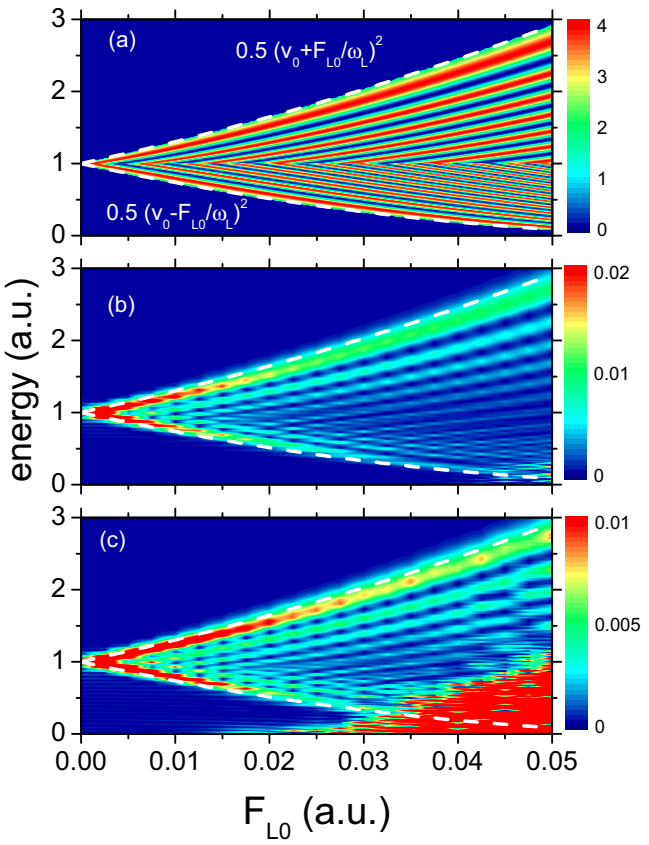

FIG. 5. Photoelectron spectra in the forward direction (in arbitrary units) calculated at different laser field strengths within (a) the SCM, (b) the SFA, and (c) the TDSE. The IR laser frequency is $\omega_L = 0.05$ and the XUV pulse parameters are $F_{X0} = 0.01, \omega_X = 1.5$, and $\tau_X = T_L$. Both XUV and IR fields are cosinelike. The classical boundaries of laser-assisted photoemission are shown with dashed lines. The high-intensity spot in the right bottom corner of (c) corresponds to ionization by the IR laser pulse alone.

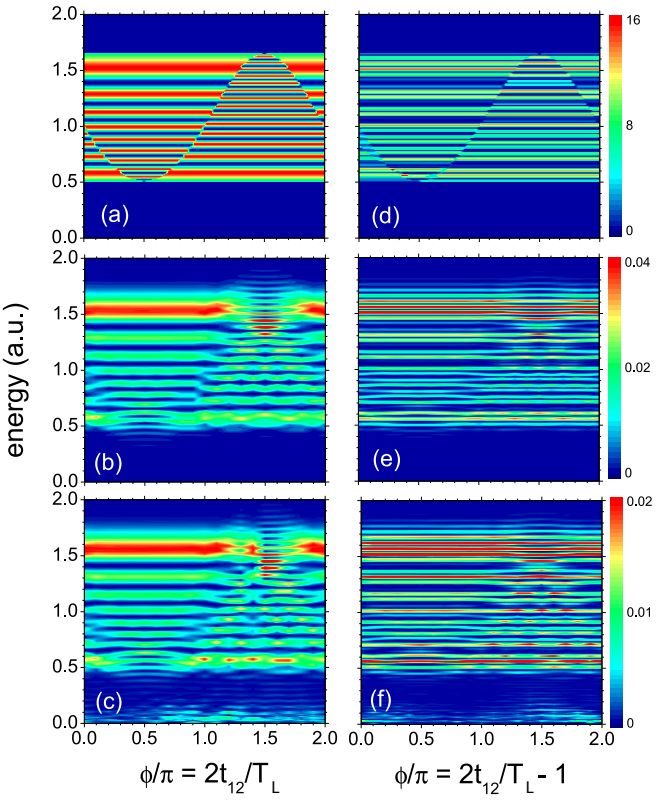

FIG. 6. Photoelectron spectra in the forward direction (in arbitrary units) as a function of the optical phase (time delay t_{12}) within (a) and (d) the SCM, (b) and (e) the SFA, and (c) and (f) the TDSE. The IR laser frequency is $\omega_L = 0.05$, $\tau_L = 7T_L$, and the XUV pulse has $F_{X0} = 0.01$, $\omega_X = 1.5$, XUV pulse duration (a)–(c) $\tau_X = T_L$ and (d)–(f) $\tau_X = 2T_L$.

the independence of the intracycle interference pattern with the time delay, except for the discontinuity in Eq. (22) for energy values equal to $E_{\rm disc} = [v_0 - A(\tau_L/2 - t_{12} - T_L/2)]^2/2$. For $t_{12} = 0$, the discontinuity is situated at $E_{\rm disc} = v_0^2/2$ since $A(\tau_L/2 - T_L/2) = 0$, as shown in Fig. 2. As t_{12} (and ϕ) varies, the discontinuity follows the shape of the vector potential. For the cases that $\phi = \pi/2$ and $3\pi/2$ the discontinuity moves to the classical boundary losing entity. For the case $\phi = \pi/2$, the separation between consecutive intracycle interference stripes is smaller for lower energies and increases as the energy grows. Contrarily, for $\phi = 3\pi/2$, energy separation between consecutive intracycle interference maxima is higher for lower energy and diminishes as energy increases. The SFA and TDSE energy distributions in Figs. 6(b) and 6(c), respectively, exhibit characteristics similar to those of the SCM. Interestingly, the discontinuity at $E_{\rm disc}$ can be clearly observed as a jump of the probability distributions for the same energy values. The remarkable resemblance between the SFA and TDSE results shows once again that the SFA is very appropriate to deal with laser-assisted photoemission processes and computationally much less demanding than solving the TDSE *ab initio*. Low-energy contributions in TDSE calculations shown in Fig. 6(c) are due to IR ionization as described before. There are two characteristics of SFA and TDSE spectra that deserve more study: (i) For $\phi \simeq \pi/2$ the energy distribution extends to lower-energy values than for other ϕ values ($E \simeq 0.5$), whereas for $\phi \simeq 3\pi/2$ it extends for higher-energy values ($E \simeq 1.5$), and (ii) the horizontal intracycle interference stripes show some structure below the above-mentioned discontinuity, i.e., $E < E_{\rm disc}$, which is absent above it, i.e., $E > E_{\rm disc}$.

When we calculate the energy distribution for an XUV pulse with duration $\tau_X = 2T_L$, our active window comprises two IR optical cycles. For the particular case of zero time delay, i.e., $t_{12} = 0$ (both IR and XUV pulses centered at the same instant of time), the vector potential from the perspective of the active window has a change of sign compared to the $\tau_X = T_L$ case, i.e., $A(t) = -A_0 \sin[\omega_L(t - t_b)]$. Therefore, for the sake of comparison, we redefine the optical phase $\phi = \omega_L t_{12} - \pi = 2\pi t_{12}/T_L - \pi$, varying the time delay t_{12} from $T_L/2$ up to $3T_L/2$. With this new definition, $\phi = 0$ corresponds to $t_{12} = T_L/2$, with the same behavior of the vector potential inside the active window. In Fig. 6(d) the SCM spectrum displays horizontal lines corresponding to the intercycle interference modulated by the intracycle pattern of Fig. 6(a). The discontinuity of the intracycle modulation can also be observed, which mirrors as a probability jump

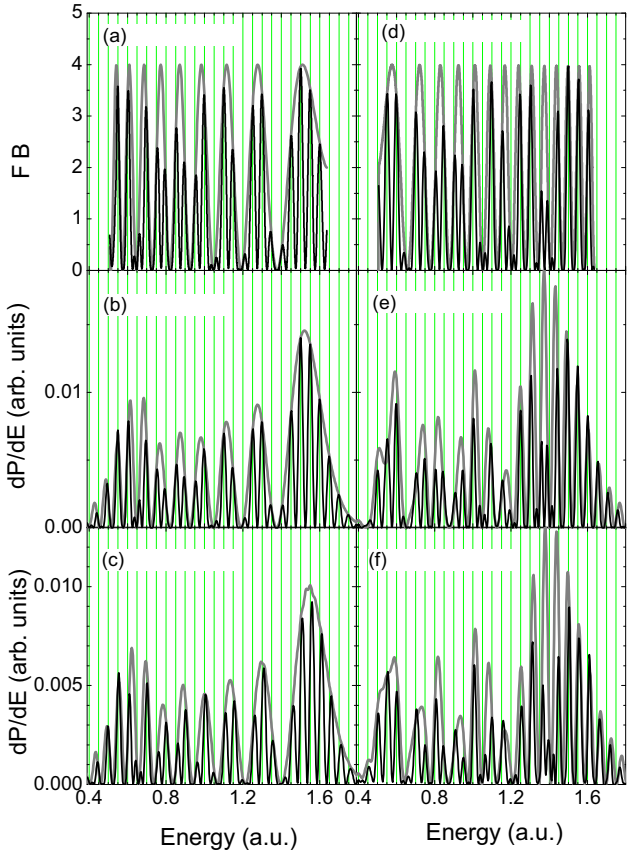

FIG. 7. Photoelectron spectra in the forward direction (in arbitrary units) for time delays t_{12} corresponding to (a)–(c) $\phi = \pi/2$ and (d)–(f) $\phi = 3\pi/2$ within (a) and (d) the SCM, (b) and (e) the SFA, and (c) and (f) the TDSE. The IR laser frequency is $\omega_L = 0.05$, $\tau_L = 7T_L$, and the XUV pulse parameters are $F_{X0} = 0.01$, $\omega_X = 1.5$, and $\tau_X = T_L$ (thick dark gray curve) and $\tau_X = 2T_L$ (thick light gray curve).

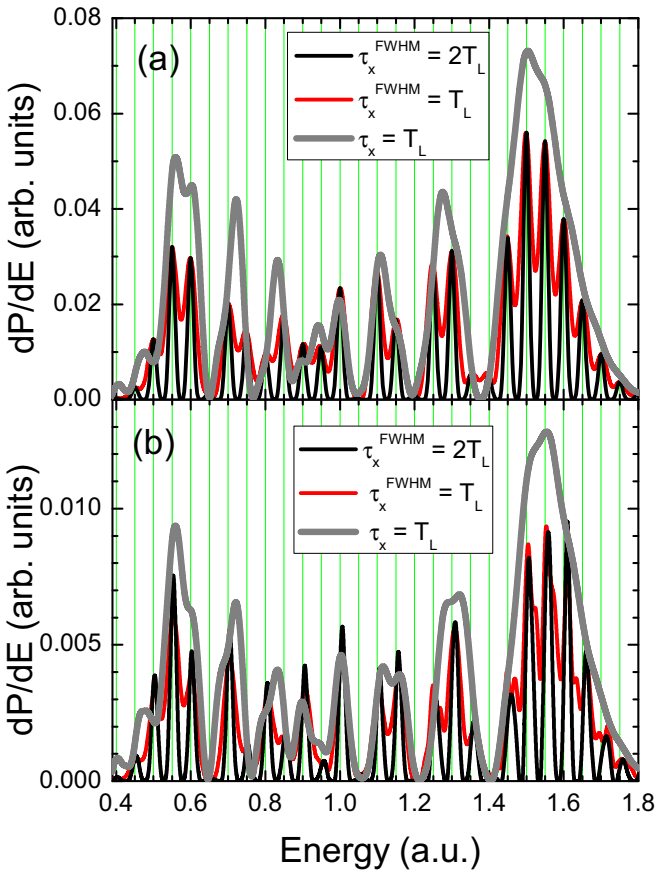

FIG. 8. Energy distribution in the forward direction calculated within (a) the SFA and (b) the TDSE. The laser duration is $\tau_L = 9T_L = 1130.97$ and the envelope function of the XUV pulse is $F_{X0}(t) = \sin^2(\pi t/\tau_X)$ with $\tau_X = 345.2$ and 690.4, which correspond to a FWHM duration of $\tau_X^{\mathrm{FWHM}} = T_L$ and $2T_L$, respectively. For completeness, we also show the intracycle momentum for the flattop XUV pulse of Fig. 3 (thick gray curve). Vertical lines depict the positions of the sidebands E_n according to Eq. (24).

for the SFA [Fig. 6(e)] and TDSE [Fig. 6(f)] too. Once again, the agreement between the SFA and TDSE is very good, with the exception of the low-energy contribution due to the ionization by the IR laser pulse in the TDSE spectrogram. By comparing the intracycle pattern for $\tau_X = T_L$ in Figs. 6(a)–6(c) to the whole interference pattern for $\tau_X = 2T_L$ in Figs. 6(d)–6(f), we see the interplay between intra- and intercycle interference, i.e., the intracycle interference pattern works as a modulation of the intercycle interference pattern (sidebands) for the active window with a duration of two optical laser cycles.

The intracycle energy distributions ($\tau_X = T_L$) in Figs. 2, 3(a), and 3(b) can be regarded as cuts of the intracycle interferograms of Figs. 6(a)–6(c), respectively. For the sake of completeness, we show also in Figs. 7(a)–7(c) the energy distribution for $\phi = \pi/2$ for $\tau_X = T_L$ and $\tau_X = 2T_L$. We observe how in all calculations [SCM, SFA, and TDSE in Figs. 7(a)–7(c), respectively] the separation of the consecutive intracycle maxima grows as the energy increases. The energy distributions for $\tau_X = 2T_L$ show a sideband structure (intercycle interference) modulated by the intracycle interference pattern. As the separation of the intracycle maxima near the lower classical limit is close to the laser photon energy $\hbar\omega_L$, it competes with the intercycle interference pattern (sidebands) for $\tau_X = 2T_L$ whose separation is also $\hbar\omega_L$. Therefore, the interplay of intra- and intercycle interference patterns gives rise to new oscillation structures of the energy distribution by ionization of the XUV pulse of duration $\tau_X = 2T_L$ assisted by the laser pulse. For example, a gross structure is observed [Figs. 7(b) and 7(c)] with a maximum at $E \simeq 0.63$ for the SFA and TDSE. The same is valid for the phase $\phi = 3\pi/2$ in Figs. 7(d)–7(f) for the SCM, SFA, and TDSE, respectively. However, in this case, the competition between intra- and intercycle interference patterns takes place close to the classical high-energy limit. Again, a grosser structure is formed, making the energy distributions similar when $\tau_X = 2T_L$ for $\phi = \pi/2$ and $\phi = 3\pi/2$. It is expected that as the active window gets wider, i.e., $\tau_X \gg T_L$, the agreement between energy spectra for $\phi = \pi/2$ and $\phi = 3\pi/2$ improves.

In the following we investigate the effect of the envelope of the XUV pulse $F_{X0}(t)$ on laser-assisted photoemission. So far, we have used the trapezoidal envelope given by Eq. (28), which

opens a well-defined active window of duration almost equal to τ_X (since it has a one-cycle ramp on and one-cycle ramp off, each of duration $T_X = 2\pi/\omega_X \ll T_L$). Now we consider an XUV pulse with squared sine envelope

$$F_{X0}(t) = \sin^2\left(\frac{\pi t}{\tau_X}\right) = \sin^2\left(\frac{\pi t}{2\tau_X^{\mathrm{FWHM}}}\right), \qquad (29)$$

where $\tau_X^{\mathrm{FWHM}} = \tau_X/2$ is the full width at half maximum (FWHM) duration of the electric field. The results for the energy distribution in the forward direction due to an XUV pulse with $\sin^2$ envelope with $\tau_X^{\mathrm{FWHM}} = T_L$ assisted by the laser pulse described in Eqs. (25) and (26) calculated within the SFA and TDSE are displayed in Figs. 8(a) and 8(b), respectively. Clearly, sidebands are modulated by the intracycle pattern given by the electron energy distribution produced by the one-cycle trapezoidal XUV pulse of Eqs. (27) and (28). When we compare these results with the energy distribution calculated with the flattop pulse of Eqs. (27) and (28), we realize that the origin of the modulations of the sidebands is due to the intracycle interference also for the $\sin^2$ XUV envelope of Eq. (29). When we double the duration of the XUV pulse, i.e., $\tau_X^{\mathrm{FWHM}} = 2T_L$, the sideband peaks are sharper because the doubles of the optical cycles are involved in the active window enhancing, consequently, the intercycle interference, giving rise to almost perfect destructive interference (the minima of the energy distribution are zero). The agreement between SFA and TDSE calculations is very good. We can say, therefore, that the envelope of the XUV pulse plays a minor role in laser-assisted photoemission and most of the conclusions derived for the flattop XUV pulse are still valid for a smooth experimental-like envelope shape.

IV. CONCLUSION

We have studied the electron emission in the forward direction produced by atomic hydrogen ionization subject to an XUV pulse in the presence of a strong infrared laser pulse with both pulses linearly polarized in the same direction. We extended the SCM developed for ATI due to an IR pulse to laser-assisted photoemission processes in XUV-IR ionization. In accordance with previous results employing the SFA and saddle-point approximation [11–13], the PE spectrum can be factorized into two contributions, one accounting for sideband's formation and the other as a modulation. As a result, we have an interference pattern of a diffraction grating in the time domain. The intercycle interference of electron trajectories from different optical cycles of the IR laser gives rise to sidebands, whereas the intracycle interference of electron trajectories born in the same optical cycle originates from a coarse-grained pattern modulating the sidebands. By comparing the outcome of ionization considering two XUV attosecond pulses separated by the laser period with only one XUV attosecond pulse, Geng *et al.* in [21] arrived at the same conclusion. We have also compared the SCM spectra with the SFA and the solution of the time-dependent Schrödinger equation calculated *ab initio* and observed good qualitative agreement. We have studied the dependence of the electron emission on the laser intensity and observed that as the IR field increases, the spectrum becomes wider and approximately bounded by the classical energy conservation rule. We conclude that the SFA is accurate to describe the photoelectron spectrum when compared to the TDSE in a wide range of parameters. Finally, we have shown that the intracycle pattern is independent of the XUV pulse duration and envelope, but exhibits a jump at a given energy as a function of the time delay between the two pulses t_{12} reproducing the profile of the laser vector potential. This smooth jump in PE spectra manifests itself as a discontinuity in models based on the saddle-point approximation, like the present SCM.

ACKNOWLEDGMENTS

This work supported was by CONICET Grants No. PIP0386, No. PICT-2012-3004, and No. PICT-2014-2363 of ANPCyT (Argentina) and the University of Buenos Aires (Grant No. UBACyT 20020130100617BA). This work was motivated by a discussion between Pablo Macri and D.G.A.

[1] M. Drescher and F. Krausz, J. Phys. B **38**, S727 (2005).
[2] E. Goulielmakis, M. Uiberacker, R. Kienberger, A. Baltuska, V. Yakovlev, A. Scrinzi, T. Westerwalbesloh, U. Kleineberg, U. Heinzmann, M. Drescher, and F. Krausz, Science **305**, 1267 (2004).
[3] P. Johnsson, J. Mauritsson, T. Remetter, A. L'Huillier, and K. J. Schafer, Phys. Rev. Lett. **99**, 233001 (2007).
[4] J. Itatani, F. Quéré, G. L. Yudin, M. Y. Ivanov, F. Krausz, and P. B. Corkum, Phys. Rev. Lett. **88**, 173903 (2002).
[5] U. Frühling, M. Wieland, M. Gensch, T. Gebert, B. Schutte, M. Krikunova, R. Kalms, F. Budzyn, O. Grimm, J. Rossbach, E. Plonjes, and M. Drescher, Nat. Photon. **3**, 523 (2009).
[6] M. Wickenhauser, J. Burgdörfer, F. Krausz, and M. Drescher, J. Mod. Opt. **53**, 247 (2006).
[7] S. Nagele, R. Pazourek, J. Feist, K. Doblhoff-Dier, C. Lemell, K. Tokési, and J. Burgdörfer, J. Phys. B **44**, 081001 (2011).
[8] S. Düsterer, L. Rading, P. Johnsson, A. Rouzée, A. Hundertmark, M. J. J. Vrakking, P. Radcliffe, M. Meyer, A. K. Kazansky, and N. M. Kabachnik, J. Phys. B **46**, 164026 (2013).
[9] M. J. Nandor, M. A. Walker, L. D. Van Woerkom, and H. G. Muller, Phys. Rev. A **60**, R1771 (1999).
[10] H. G. Muller, Phys. Rev. A **60**, 1341 (1999).
[11] A. K. Kazansky and N. M. Kabachnik, J. Phys. B **43**, 035601 (2010).
[12] A. K. Kazansky, I. P. Sazhina, and N. M. Kabachnik, Phys. Rev. A **82**, 033420 (2010).
[13] S. Bivona, G. Bonanno, R. Burlon, and C. Leone, Laser Phys. **20**, 2036 (2010).
[14] A. Maquet and R. Taïeb, J. Mod. Opt. **54**, 1847 (2007).
[15] A. Jiménez-Galán, L. Argenti, and F. Martín, New J. Phys. **15**, 113009 (2013).
[16] R. Taïeb, A. Maquet, and M. Meyer, J. Phys.: Conf. Ser. **141**, 012017 (2008).
[17] N. M. Kroll and K. M. Watson, Phys. Rev. A **8**, 804 (1973).
[18] J. M. Schins, P. Breger, P. Agostini, R. C. Constantinescu, H. G. Muller, G. Grillon, A. Antonetti, and A. Mysyrowicz, Phys. Rev. Lett. **73**, 2180 (1994).

[19] D. G. Arbó, K. L. Ishikawa, K. Schiessl, E. Persson, and J. Burgdörfer, Phys. Rev. A **81**, 021403 (2010).
[20] D. G. Arbó, K. L. Ishikawa, K. Schiessl, E. Persson, and J. Burgdörfer, Phys. Rev. A **82**, 043426 (2010).
[21] J.-W. Geng, L.-Y. Peng, S.-N. Song, and Q. Gong, Phys. Rev. A **88**, 053418 (2013).
[22] X. M. Tong and S. I. Chu, Chem. Phys. **217**, 119 (1997).
[23] X.-M. Tong and S.-I. Chu, Phys. Rev. A **61**, 031401 (2000).
[24] X. M. Tong and C. D. Lin, J. Phys. B **38**, 2593 (2005).
[25] O. Schöller, J. S. Briggs, and R. M. Dreizler, J. Phys. B **19**, 2505 (1986).
[26] A. Messiah, *Quantum Mechanics* (North-Holland, New York, 1965), Vol. II.
[27] S. Dionissopoulou, T. Mercouris, A. Lyras, and C. A. Nicolaides, Phys. Rev. A **55**, 4397 (1997).
[28] D. Wolkow, Z. Phys. **94**, 250 (1935).
[29] R. Della Picca, J. Fiol, and P. D. Fainstein, J. Phys. B **46**, 175603 (2013).
[30] R. Della Picca, A. A. Gramajo, C. R. Garibotti, S. D. López, and D. G. Arbó, Phys. Rev. A **93**, 023419 (2016).
[31] M. Meyer, D. Cubaynes, P. O'Keeffe, H. Luna, P. Yeates, E. T. Kennedy, J. T. Costello, P. Orr, R. Taïeb, A. Maquet, S. Düsterer, P. Radcliffe, H. Redlin, A. Azima, E. Plönjes, and J. Feldhaus, Phys. Rev. A **74**, 011401(R) (2006).
[32] C. C. Chirilă and R. M. Potvliege, Phys. Rev. A **71**, 021402(R) (2005).
[33] P. B. Corkum, N. H. Burnett, and M. Y. Ivanov, Opt. Lett. **19**, 1870 (1994).
[34] M. Ivanov, P. B. Corkum, T. Zuo, and A. Bandrauk, Phys. Rev. Lett. **74**, 2933 (1995).
[35] M. Lewenstein, K. C. Kulander, K. J. Schafer, and P. H. Bucksbaum, Phys. Rev. A **51**, 1495 (1995).
[36] A. K. Kazansky and N. M. Kabachnik, J. Phys. B **42**, 121002 (2009).
[37] D. G. Arbó, K. I. Dimitriou, E. Persson, and J. Burgdörfer, Phys. Rev. A **78**, 013406 (2008).
[38] X. Xie, S. Roither, D. Kartashov, E. Persson, D. G. Arbó, L. Zhang, S. Gräfe, M. S. Schöffler, J. Burgdörfer, A. Baltuška, and M. Kitzler, Phys. Rev. Lett. **108**, 193004 (2012).